1
Spinmotive force

Jun'ichi Ieda and Sadamichi Maekawa

1.1 Introduction

This chapter overviews "spinmotive force" (SMF), which is an emerging concept that is responsible for generating spin current and electric voltage in magnetic conductors. The SMF is mediated by the exchange interaction between conduction-electron spin and magnetization and thus has the same roots as spin-transfer torque (STT) [1,2] (i.e., they are two sides of a coin). Whereas STT is responsible for the *angular-momentum-transfer* between spin current and magnetization, SMF enables the *energy-transfer* in the interacting system. Therefore, SMF is expected to give rise to an important contribution to energy management in future spintronics applications.

Motivated by the experimental demonstration of the STT driving a domain wall (DW) in a ferromagnetic nanowire in the early 2000's [3], the implementation of SMF in a similar system and its magnetic memory device applications were proposed in 2006 [4]. Soon after, the general aspect of the SMF was clarified in terms of a concept of the accumulation of Berry phase [5] by pointing out that SMF can be regarded as a generalization of Faraday's law of induction to include the electron's spin degree of freedom [6]. Since then, a series of experimental demonstrations [7–15] and theoretical investigations [16–46] of the SMF effects have appeared.

Below we list some striking features of the SMF:

- In contrast to the inductive electromotive force (EMF) where the time variation of magnetic flux is required, static magnetic fields can generate electric voltages.
- As a new source for an electric voltage the conversion rate is given by fundamental constants apart from the spin polarization of ferromagnetic materials, enabling efficient energy conversion.
- The SMF provides for a powerful tool for exploring the dynamics and the nature of magnetic textures such as domain walls, magnetic vortices, and skyrmions.
- Active devices that use this effect can operate with zero stand-by power and their efficient power conversion between the magnetic and electric systems provides a unique functionality in magnetic nanostructures.

As an introduction to the SMF, we select several topics ranging from the basic concepts to recent experimental progress. Some potential applications of the SMF will also be discussed from a theoretical viewpoint.

1.2 Description of spinmotive force

This section describes the SMF from various viewpoints. After some retrospective remarks, we start with a simple argument based on the conservation laws to deduce the existence of the SMF. To this end and for simplicity, we neglect in this section all the dissipation process (except in Fig. 1.2). Next we explain the connection to the Berry phase. Finally, we briefly introduce the spin electromagnetic fields and describe it with a numerical approach.

1.2.1 Historical remarks

The earlier work related to the SMF (before the discovery of the STT effect) occurred repeatedly but quite independently in different contexts. In 1977, Korenmann *et al.* [47] constructed a theory of the spin fluctuation in itinerant ferromagnets in which they first wrote down the widely quoted expressions for spin electromagnetic fields. These fields, however, played less important roles in their formalism and they did not identify the SMF. A decade later, Volovik [48] studied a paradox in the linear momentum of the coherent magnetization motion that couples to the incoherent fermionic excitations and re-derived the same spin electromagnetic fields implicated to restore conservation of linear momentum[1]. Technically, however, no measurable SMF was expected because the only internal magnetic energy (exchange stiffness) was incorporated as the source of total energy. Berger [49] was the first to insist that a precessing DW could generate an electric voltage, regarding it as a ferromagnetic analogue of the AC Josephson effect. Stern [5] first identified the possibility of such a spin version of the EMF in terms of the Berry phase in a nonmagnetic ring with a nonuniform magnetic field where the net electrical voltage vanishes after spin averaging. Thus, materials with a finite spin polarization P are required to convert the pure spin force to a measurable electrical voltage.

1.2.2 Conservation laws

An instructive example involving the SMF is a single DW in a conducting ferromagnetic nanowire with only uniaxial anisotropy. When we apply a magnetic field H along the easy axis of the wire a positive or negative Zeeman energy shift arises for each of the magnetic domains separated by the DW. Next, we consider that conduction electrons couple to the magnetic system, thereby allowing the exchange of energy and angular momentum. In the presence of a magnetic field, the total Zeeman energy of the nanowire depends on the DW position, and the magnetic energy changes when the DW moves with the velocity v_{DW}. The rate of change in magnetic energy per unit area of wire cross section is given by $-2\mu_0 M_{\mathrm{s}} H v_{\mathrm{DW}}$, where μ_0 is the magnetic constant and M_{s} is the saturation magnetization. Here we employ STT to drive a DW[2]. Due to conservation of angular momentum, the rate of change in angular momentum carried by the spin polarized current and the rate of change of the localized moment must balance leading to a relation between the DW velocity v_{DW} and the applied current density J as, $v_{\mathrm{DW}} = -g\mu_{\mathrm{B}} PJ/(2eM_{\mathrm{s}})$, where g is the Landé g factor, μ_{B} is the Bohr

[1] Note that the STT term already appeared in Eq. (10) of Ref. [48].

[2] Without energy dissipation, the DWs do not move along the wire due to a relaxation process.

magneton, $e > 0$ is the elementary charge and the spin polarization P is defined by the spin-dependent conductivity σ_s ($s = \uparrow, \downarrow$) as $P = (\sigma_\uparrow - \sigma_\downarrow)/(\sigma_\uparrow + \sigma_\downarrow)$. This is the DW velocity due to the STT effect [3]. Conservation of energy requires the rate of the magnetic energy change is balanced by a work done on the current J (per unit time and area) as $-2\mu_0 M_\mathrm{s} H v_\mathrm{DW} + JV = 0$, where V is the induced electric voltage. Using the STT current-velocity relation for v_DW we obtain

$$V = -\frac{Pg\mu_\mathrm{B}}{e}\mu_0 H. \tag{1.1}$$

The sign of the SMF, which ultimately depends on the definition of a measurement setup, is specified by a spin version of Lenz's law. In other words, the polarity of the induced voltage is determined by the current it must drive to oppose to the applied current and thereby restore the original DW position via the STT effect. For the field-induced DW the voltage drop develops along the direction of DW motion[3]. Equation (1.1) gives a simple conversion rate between the input field and output voltage as $\simeq P \times 100\ \mu\mathrm{V/T}$.

The SMF associated with field-driven DW dynamics was measured for the first time by Yang *et al.* who used a modulated-drive-field technique in a 500-nm-wide, 20-nm-thick, and 35-μm-long permalloy nanowire [7, 24]. By using Eq. (1.1), they determined the spin polarization of the permalloy sample to be $P \sim 0.85$. Reference [50] further discusses the SMF induced by DW motion.

1.2.3 Time dependent spin Berry phase

To obtain Eq. (1.1), we only assume conservation of angular momentum and energy between the conduction electrons and the magnetization. We now show that Eq. (1.1) is identical to the general expression of the SMF [6],

$$V = \frac{P\hbar}{e}\frac{d\gamma_\mathrm{s}}{dt}, \tag{1.2}$$

where $\hbar$ is the Planck's constant divided by 2π and γ_s is the so-called Berry phase associated with the spin degree of freedom of an electron.

The Berry phase reflects the geometric aspects of the system in general, which plays an important role in the understanding of phenomena in recent spintronics, such as the quantum spin Hall effect and the anomalous Hall effect [51]. Here it is related to the solid angle Ω subtended by the trajectory of the spin direction in spin space as $\gamma_\mathrm{s} = -\Omega/2$ [52]. To calculate the SMF, the time variation of the solid angle is needed and, for a DW under a uniform magnetic field H, this is given by twice the Larmor precession frequency: $d\Omega/dt = 2\gamma H$ where γ is the gyromagnetic ratio. By using $\gamma = g\mu_\mathrm{B}\mu_0/\hbar$, one can show that Eq. (1.1) is identical to Eq. (1.2). This expression is a generalization of Faraday's law of induction since the Berry phase associated with the charge degree of freedom (the Aharonov–Bohm phase) is given by $\gamma_\mathrm{e} = (-e/\hbar)\Phi$ where Φ is the magnetic flux and Eq. (1.2) with γ_e reproduces the conventional expression.

[3]For $P < 0$ the voltage polarity reverses because the STT DW velocity changes the sign.

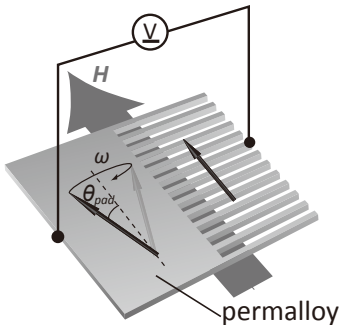

Fig. 1.1 Schematic illustration of the permalloy comb sample used in Ref. [9].

Another simple example where the spin Berry phase can be obtained analytically is a system of two precessing macro spins. Consider a single ferromagnet film with two uniform magnetic domains that precess about the applied field H with the frequency ω but different corn angles, θ_i $(i = 1, 2)$. The magnetization direction between two domains continuously changes as in a DW. In this case, the time derivative of the spin Berry phase acquired by a conduction electron traversing the film is given by

$$V = \frac{P\hbar\omega}{2e}(\cos\theta_2 - \cos\theta_1). \tag{1.3}$$

If $\theta_1 \neq \theta_2$ a voltage appears between two contacts attached to each side of the film.

This situation is experimentally realized in a comb-shaped permalloy thin film, as shown in Fig. 1.1 [9]. Due to the shape magnetic anisotropy, the wide region (pad) and narrow region (wire) of the single film sample have different resonance conditions for a fixed applied microwave frequency ω. This fact enables the selective excitation of the ferromagnetic resonance (FMR) of the pad or wire. For example, if the pad resonance condition is fulfilled, the cone angle of the pad is finite, $\theta_1 = \theta_{\rm pad} \neq 0$, and that of the wire is $\theta_2 = \theta_{\rm wire} = 0$. For $\theta_{\rm pad} \ll 1$, we expand Eq. (1.3) to obtain

$$V \simeq \frac{P\hbar\omega}{4e}\theta_{\rm pad}^2, \tag{1.4}$$

which is proportional to the applied microwave power. On the other hand, when the wire is excited resonantly the voltage sign should be reversed. These predictions are confirmed experimentally and numerically [9], demonstrating the continuous generation of SMF that can convert ac magnetic fields to dc electrical voltages.

Equation (1.2) is also evaluated for a sliding motion of a chiral soliton lattice [35].

1.2.4 Spin electromagnetic fields

As we noted above, the SMF can be regarded as a spin version of Faraday's law of induction. Thus one may expect a local expression for a spin version of electromagnetic fields. Generally, appearance of an EMF requires a nonconservative force acting on

electrons; a force that cannot be described as a spatial gradient of any potentials. An EMF is given by

$$V = \frac{1}{-e} \oint \boldsymbol{f} \cdot d\boldsymbol{x}, \tag{1.5}$$

where the integral $\oint d\boldsymbol{x}$ is taken along an electric circuit through which the electron passes, and $\boldsymbol{f}$ is the force that acts on the electron. The right-hand side of Eq. (1.5) corresponds to the total energy supplied to the electron (divided by $-e$) while the electron travels and conservative forces do not contribute to this quantity.

In electromagnetism, the time-derivative of a U(1) vector potential gives rise to a nonconservative electric field, resulting in an inductive EMF. This EMF is described by Faraday's law of induction (i.e., the time derivative of a magnetic flux) and its energy source is the applied electromagnetic fields $\boldsymbol{E}$ and $\boldsymbol{B}$, which couple to the electrons via the Lorentz force $\boldsymbol{f}_e = -e(\boldsymbol{E} + \boldsymbol{v} \times \boldsymbol{B})$, where $\boldsymbol{v}$ is the electron velocity.

Conversely, the spin degree of freedom of the electron in a ferromagnet couples to the magnetization via the exchange interaction. Through this interaction the electron can receive magnetic energy from the magnetization, which can be an additional source for the EMF (1.5). The exchange interaction with the magnetization acts as a SU(2) potential for the electrons, giving rise to a spin-dependent nonconservative force $\boldsymbol{f}_\pm$ acting on the electrons,

$$\boldsymbol{f}_\pm = -e\left[\pm\boldsymbol{\mathcal{E}} + \boldsymbol{v} \times (\pm\boldsymbol{\mathcal{B}})\right], \tag{1.6}$$

where $+$ $(-)$ corresponds to the majority (minority) electrons, and the so-called spin electric and spin magnetic fields, $\boldsymbol{\mathcal{E}}$ and $\boldsymbol{\mathcal{B}}$, are given by

$$\mathcal{E}_i = \frac{\hbar}{2e}\boldsymbol{m} \cdot \left(\frac{\partial \boldsymbol{m}}{\partial t} \times \frac{\partial \boldsymbol{m}}{\partial x_i}\right), \quad \mathcal{B}_i = -\epsilon_{ijk}\frac{\hbar}{4e}\boldsymbol{m} \cdot \left(\frac{\partial \boldsymbol{m}}{\partial x_j} \times \frac{\partial \boldsymbol{m}}{\partial x_k}\right), \tag{1.7}$$

where $\boldsymbol{m}$ denotes the unit vector of the magnetization direction, ϵ_{ijk} is the Levi–Civita symbol, and the dot and cross products are taken over the vector components of $\boldsymbol{m}$. We will see the derivation of Eqs. (1.6) and (1.7) in the next section.[4]

This spin electric field $\boldsymbol{\mathcal{E}}$ is nonzero when magnetization depends on both time and space. Such conditions are fulfilled for the field-induced DW motion and the spatially modulated FMR as seen in the previous subsections. By integrating $\boldsymbol{\mathcal{E}}$ for the particular cases we recover Eqs. (1.1) and (1.3) respectively.

The spin magnetic field $\boldsymbol{\mathcal{B}}$ is produced by a noncoplanar magnetization configuration. The Lorentz-type force $-e[\boldsymbol{v} \times (\pm\boldsymbol{\mathcal{B}})]$ gives rise to the transverse conductivity. This effect is called the anomalous Hall effect due to the spin chirality [53–56].

The forces on the majority spin and minority spin are opposite and the net force acting on electrons are averaged over the spin bands. This implies that a force exerted on electrons is associated with the spin polarization P of the ferromagnet[5] as

$$\boldsymbol{f}_{\rm nc} = -\frac{P\hbar}{2}\boldsymbol{m} \cdot \left(\frac{\partial \boldsymbol{m}}{\partial t} \times \nabla \boldsymbol{m}\right). \tag{1.8}$$

This is the nonconservative force exerted on electrons from dynamical magnetization.

[4]Note that the use of the unit vector $\boldsymbol{n} \equiv -\boldsymbol{m}$ instead of the magnetization vector $\boldsymbol{m}$ reverses the overall signs of Eqs. (1.7) as adopted in some publications [27, 37].

[5]More accurate treatments involving the spin diffusion with $\boldsymbol{f}_\pm$ are given in Refs. [19, 20, 22–27].

1.2.5 Numerical approach

We see that the SMF reflects the local magnetization texture. In reality, the magnetization dynamics show complex spatiotemporal profiles that depend on sample geometry, applied magnetic fields, and other conditions. Tracing in detail the time evolution of the magnetization structure requires a numerical analysis using the finite element method. The numerical analysis of the magnetization dynamics is referred to as micromagnetics. For this purpose we use the open-access cords such as the object oriented micromagnetic framework (OOMMF) [57].

Numerical methods for evaluating SMFs was first developed by Ohe *et al.* [21], who applied their method to the system of a gyrating magnetic vortex core. The procedure is as follows: First, based on information of the magnetization obtained by micromagnetics, the spin-electric field $\boldsymbol{\mathcal{E}}$ is calculated at every time step. In electron equilibrium, the nonconservative force derived above is balanced by a conservative force [a U(1) electric field] $\boldsymbol{E}_{\rm c} = -\nabla V$ [i.e., $\boldsymbol{f}_{\rm nc} + (-e)\boldsymbol{E}_{\rm c} = \boldsymbol{0}$]. Finally, using this relation the Poisson equation

$$\Delta V = -\frac{1}{e}\nabla \boldsymbol{f}_{\rm nc}, \tag{1.9}$$

is numerically solved under certain boundary conditions, which enables a quantitative evaluation of the SMF in a given ferromagnetic nanostructure.

Figure 1.2 shows an example of numerical simulations of DW motion and the associated voltage profile in a permalloy nanowire. Here the moving DW exhibits a complex two-dimensional magnetization configuration [Fig.1.2(a)] and the associated potential distribution changes significantly around the DW [Fig. 1.2(b)]. By monitoring the potential difference between the electrodes attached to any two positions of the sample, the voltage signal due to SMF can be detected in real time. For the simulation result shown in Fig. 1.2, the time-averaged voltage drop is calculated to be ~ 0.9 μV, which is consistent with Eq. (1.1) with $\mu_0 H = 14$ mT and $P = 0.6$. A more detailed numerical analysis of the SMF generated by DW motion is found in Ref. [38].

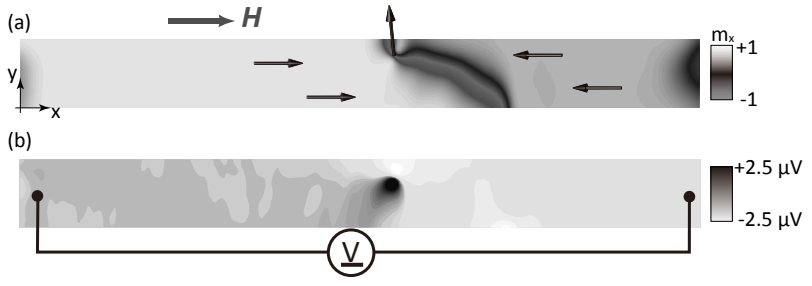

Fig. 1.2 Numerical results for field-induced DW motion in a permalloy nanowire (1000×100 nm^2). (a) Snapshot of magnetization profile (m_x component displayed in gray scale). Solid arrows represent local magnetization directions. (b) The electric potential profile associated with panel (a). Here we use $\mu_0 H = 14$ mT, $\mu_0 M_{\rm s} = 1$ T, $P = 0.6$, the Gilbert damping constant is 0.01, and the exchange stiffness is 1.3×10^{-11} J/m.

1.3 Theory of spinmotive force

In this section, we derive the spin electromagnetic fields (1.7) and their extensions. There are several practically equivalent ways to do this, for example, in terms of the Berry curvatures [6,24,36], the Onsager reciprocal relations [17,19,44], and the linear response to magnetization dynamics [27,37]. In this section, to clarify the origin of the SMF, we introduce an approach based on the equation of motion [28].

1.3.1 s–d model

We begin with the Hamiltonian of the s–d model[6] for the conduction electrons in a ferromagnetic material,

$$\mathcal{H} = \frac{\boldsymbol{p}^2}{2m_\mathrm{e}} + J_\mathrm{ex}\boldsymbol{\sigma}\cdot\boldsymbol{m}, \tag{1.10}$$

where $\boldsymbol{p}$ and m_e are the linear momentum operator and electron mass, respectively. The second term represents the exchange interaction, with $J_\mathrm{ex}(>0)$ being the exchange coupling energy, $\boldsymbol{\sigma}$ being the Pauli matrices indicating the electron-spin operator defined in the laboratory frame, and $\boldsymbol{m}$ being the unit vector of the magnetization direction. The magnetization generally depends on time and space.

By the correspondence principle, a quantum-mechanical "force" operator acting on the conduction electrons is given by the Heisenberg equation of motion

$$\boldsymbol{f} = \frac{m_\mathrm{e}}{i\hbar}[\boldsymbol{v},\mathcal{H}] + m_\mathrm{e}\dot{\boldsymbol{v}}, \tag{1.11}$$

where $\boldsymbol{v} = [\boldsymbol{r},\mathcal{H}]/(i\hbar) = \boldsymbol{p}/m_\mathrm{e}$ is the velocity operator and the dot denotes the partial derivative with respect to time, $\dot{\boldsymbol{v}} \equiv \partial\boldsymbol{v}/\partial t$. Next, the expectation value of the force operator is determined by that of the spin operator $\langle\boldsymbol{\sigma}\rangle$ and the magnetization as

$$\langle\boldsymbol{f}\rangle = -J_\mathrm{ex}\langle\boldsymbol{\sigma}\rangle\cdot\nabla\boldsymbol{m}. \tag{1.12}$$

For uniform magnetization ($\nabla\boldsymbol{m} = \boldsymbol{0}$), the force acting on the electron spin vanishes, so no SMF is generated in the system described by the Hamiltonian (1.10).

Let us now consider the case in which nonuniform magnetization is in motion. The dynamics of $\boldsymbol{m}$ is described by the Landau–Lifshitz–Gilbert (LLG) equation:

$$\dot{\boldsymbol{m}} = -\gamma\boldsymbol{m}\times\boldsymbol{H}_\mathrm{eff} + \alpha\boldsymbol{m}\times\dot{\boldsymbol{m}}, \tag{1.13}$$

where α is the Gilbert damping constant and the effective magnetic field is defined as

$$\boldsymbol{H}_\mathrm{eff} = -\frac{1}{\mu_0 M_\mathrm{s}}\frac{\delta F[\boldsymbol{m}]}{\delta\boldsymbol{m}}, \tag{1.14}$$

where $F[\boldsymbol{m}]$ is the free energy of the ferromagnet, which comprises the exchange, anisotropy, dipole, and Zeeman energies. By solving the LLG equation, Eq. (1.12) is evaluated at each point and time.

[6] An approach based on the Stoner model was developed in Ref. [6] and in the 1st ed. of this chapter.

1.3.2 Adiabatic contribution

Let us calculate the expectation value of the conduction-electron spin. To this end, by a local gauge transformation in the spin space, we rotate the spin quantization axis, which is originally the z axis of the laboratory frame, $\hat{\boldsymbol{z}}$, so that it aligns with the magnetization $\boldsymbol{m}$. The direction $\boldsymbol{m}$ in the laboratory frame is specified by the Euler angles (θ, φ) as $\boldsymbol{m} = {}^t(\sin\theta\cos\varphi, \sin\theta\sin\varphi, \cos\theta)$. By using a unitary matrix $U \equiv e^{i\frac{\theta}{2}\sigma_y} e^{i\frac{\varphi}{2}\sigma_z}$, the Hamiltonian (1.10) is transformed as follows,

$$\mathcal{H}' = \frac{1}{2m_{\rm e}}(\boldsymbol{p} + \boldsymbol{\mathcal{A}})^2 + J_{\rm ex}\sigma_z + \mathcal{A}_0, \tag{1.15}$$

where the SU(2) gauge potentials (connection 1-forms)

$$\boldsymbol{\mathcal{A}} \equiv \frac{\hbar}{i} U \nabla U^\dagger = \frac{\hbar}{2}(\sin\theta\nabla\varphi\sigma_x - \nabla\theta\sigma_y - \cos\theta\nabla\varphi\sigma_z), \tag{1.16}$$

$$\mathcal{A}_0 \equiv \frac{\hbar}{i} U \dot{U}^\dagger = \frac{\hbar}{2}(\sin\theta\dot{\varphi}\sigma_x - \dot{\theta}\sigma_y - \cos\theta\dot{\varphi}\sigma_z) \tag{1.17}$$

arise for nonuniform and time-varying magnetization, respectively. Compared with the original Hamiltonian (1.10), the exchange interaction becomes diagonal in the new local frame spanned by $\hat{\boldsymbol{x}}' = {}^t(\cos\theta\cos\varphi, \cos\theta\sin\varphi, -\sin\theta)$, $\hat{\boldsymbol{y}}' = {}^t(-\sin\varphi, \cos\varphi, 0)$, and $\hat{\boldsymbol{z}}' = \boldsymbol{m}$ whereas, to compensate, $\boldsymbol{\mathcal{A}}$ and $\mathcal{A}_0$ have off-diagonal components.[7]

To proceed, it is convenient to introduce the unitary matrix $U_{\rm O(3)} \equiv (\hat{\boldsymbol{x}}', \hat{\boldsymbol{y}}', \hat{\boldsymbol{z}}')^\dagger$, which changes the basis from $\{\hat{\boldsymbol{x}}, \hat{\boldsymbol{y}}, \hat{\boldsymbol{z}}\}$ to $\{\hat{\boldsymbol{x}}', \hat{\boldsymbol{y}}', \hat{\boldsymbol{z}}'\}$. One can show that $U(\boldsymbol{\sigma}\cdot\boldsymbol{a})U^\dagger = \boldsymbol{\sigma}\cdot\left(U_{\rm O(3)}\boldsymbol{a}\right)$ for a three-dimensional vector $\boldsymbol{a}$. Collecting the spin-dependent terms of the new Hamiltonian (1.15) we obtain

$$\mathcal{H}_{\rm ex} = J_{\rm ex}\boldsymbol{\sigma}\cdot\left\{\left[1 - \frac{\hbar}{2J_{\rm ex}}\left(\cos\theta\dot{\varphi} + \frac{1}{2}\left(\boldsymbol{v}\cdot\cos\theta\nabla\varphi + \cos\theta\nabla\varphi\cdot\boldsymbol{v}\right)\right)\right]\boldsymbol{m}' - \frac{\hbar}{2J_{\rm ex}}\left[(\boldsymbol{m}\times\dot{\boldsymbol{m}})' + \frac{1}{2}\left[\boldsymbol{v}\cdot(\boldsymbol{m}\times\nabla\boldsymbol{m})' + (\boldsymbol{m}\times\nabla\boldsymbol{m})'\cdot\boldsymbol{v}\right]\right]\right\}, \tag{1.18}$$

where $\boldsymbol{m}' = U_{\rm O(3)}\boldsymbol{m} = {}^t(0,0,1)$ and $(\boldsymbol{m}\times\dot{\boldsymbol{m}})' = U_{\rm O(3)}(\boldsymbol{m}\times\dot{\boldsymbol{m}}) = {}^t(-\sin\theta\dot{\varphi}, \dot{\theta}, 0)$ denotes the vectors represented in the rotated frame of reference. Equation (1.18) shows that the conduction spin interacts not only with the longitudinal field parallel to the instantaneous magnetization direction $\boldsymbol{m}'$ but with the transverse fields being proportional to $(\boldsymbol{m}\times\dot{\boldsymbol{m}})'$ and $(\boldsymbol{m}\times\nabla\boldsymbol{m})'$.

Now we assume smooth and slow variations of the magnetization satisfying $|\dot{\boldsymbol{m}}| \ll \hbar^{-1}J_{\rm ex}$ and $|(\boldsymbol{v}_{\rm F}\cdot\nabla)\boldsymbol{m}| \ll \hbar^{-1}J_{\rm ex}$, with $\boldsymbol{v}_{\rm F}$ being the Fermi velocity of the conduction electrons. These *adiabatic* conditions allow the systematic expansion with respect to $J_{\rm ex}$ of the problem described by Hamiltonian (1.18). Taking the leading contributions is referred to as the adiabatic approximation.

[7] Such gauge fields associated with the coordinate transformation are called *pure gauges* and do not produce any new forces by themselves [58].

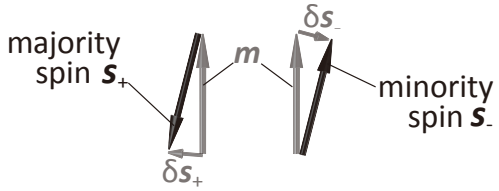

Fig. 1.3 The normalized expectation value of the spin, $\boldsymbol{s}_\pm$, and the magnetization unit vector $\boldsymbol{m}$. When $\boldsymbol{m}$ depends on time or when the electron moves in the spatially nonuniform $\boldsymbol{m}$, the directions $\boldsymbol{s}_\pm$ deviate from $\mp\boldsymbol{m}$ by $\delta\boldsymbol{s}_\pm$, as indicated by the small arrows.

The dynamics of conduction-electron spin obeys the Heisenberg equation

$$\frac{d}{dt}\boldsymbol{\sigma} = \frac{1}{i\hbar}[\boldsymbol{\sigma}, \mathcal{H}_{\rm ex}], \tag{1.19}$$

and the instantaneous one-electron eigenstates with momentum $\boldsymbol{k}$, $|\boldsymbol{k}\pm\rangle$ can be constructed, where $+$ $(-)$ denotes the majority (minority) spin state. The expectation value of the spin operator up to $O(J_{\rm ex}^{-1})$ is then given by (in the original basis)

$$\boldsymbol{s}_\pm \equiv \langle \boldsymbol{k}\pm|\boldsymbol{\sigma}|\boldsymbol{k}\pm\rangle \simeq \pm\left[-\boldsymbol{m} + \frac{\hbar}{2J_{\rm ex}}(\boldsymbol{m}\times\dot{\boldsymbol{m}}) + \frac{\hbar}{2J_{\rm ex}}[\boldsymbol{m}\times(\boldsymbol{v}_k\cdot\nabla)\boldsymbol{m}]\right]. \tag{1.20}$$

Equation (1.20) indicates that, when the magnetization dynamics is induced ($\dot{\boldsymbol{m}} \neq \boldsymbol{0}$) or when the electron flows in a nonuniform magnetization texture ($\boldsymbol{v}_k\cdot\nabla)\boldsymbol{m} \neq \boldsymbol{0}$, the direction of the spin expectation value slightly deviates from the magnetization axis ($\mp\boldsymbol{m}$), giving rise to the misalignment of the conduction-electron spin $\delta\boldsymbol{s}_\pm$, as shown in Fig. 1.3. Substituting Eq. (1.20) into Eq. (1.12), we obtain the spin force as

$$\boldsymbol{f}_\pm \equiv \langle \boldsymbol{k}\pm|\boldsymbol{f}|\boldsymbol{k}\pm\rangle = \mp e(\boldsymbol{\mathcal{E}} + \boldsymbol{v}_k\times\boldsymbol{\mathcal{B}}), \tag{1.21}$$

where the spin electric and magnetic fields are given by

$$\boldsymbol{\mathcal{E}} = \frac{\hbar}{2e}\boldsymbol{m}\cdot(\dot{\boldsymbol{m}}\times\nabla\boldsymbol{m}), \tag{1.22}$$

$$\boldsymbol{\mathcal{B}} = \frac{\hbar}{2e}\begin{bmatrix} \boldsymbol{m}\cdot\left(\frac{\partial\boldsymbol{m}}{\partial z}\times\frac{\partial\boldsymbol{m}}{\partial y}\right) \\ \boldsymbol{m}\cdot\left(\frac{\partial\boldsymbol{m}}{\partial x}\times\frac{\partial\boldsymbol{m}}{\partial z}\right) \\ \boldsymbol{m}\cdot\left(\frac{\partial\boldsymbol{m}}{\partial y}\times\frac{\partial\boldsymbol{m}}{\partial x}\right) \end{bmatrix}. \tag{1.23}$$

These fields are the adiabatic contribution to the spin electromagnetic fields.

Note that omitting the transverse fields in Eq. (1.18) results in no misalignment $\delta\boldsymbol{s}_\pm = \boldsymbol{0}$ and the null result[8]. The transverse parts of the spin gauge fields represent the generators of translation with respect to the magnetization texture,[9] and the resulting misalignment is the key ingredient in the process transferring both angular momentum (STT)[10] and energy (SMF) between magnetization and conduction spin.

[8]The role of the transverse fields on the local band theory was studied in Ref. [47].

[9]The detailed arguments are found in the 1st ed. of this chapter.

[10]The derivation of the STT term along with the present scenario is explained in Ref. [59].

1.3.3 Nonadiabatic contribution

Next we extend the spin electric field (1.22) to include the nonadiabatic correction due to spin-flip process. Duine [17] and Tserkovnyak and Mecklenburg [19] introduced such a nonadiabatic contribution on the basis of the Onsager reciprocal relation between the dynamics of magnetization and the conduction electrons as follows:

$$\boldsymbol{\mathcal{E}} = \beta \frac{\hbar}{2e} \dot{\boldsymbol{m}} \cdot \nabla \boldsymbol{m}, \tag{1.24}$$

where β is a dimensionless phenomenological parameter. Shibata and Kohno [27] obtained the same expression from a linear response approach by carefully accounting for spin-relaxation effects.

Here we derive the above expression by extending the preceding argument. In the derivation of the spin-dependent force (1.21), we assumed that electron spin aligns the instantaneous field direction adiabatically, resulting in the expectation value

$$\boldsymbol{s}_{\pm} = \mp \boldsymbol{m} + \delta \boldsymbol{s}_{\pm}, \tag{1.25}$$

where the second term on the right-hand side represents the deviation from $\mp \boldsymbol{m}$. In general, $\delta \boldsymbol{s}_{\pm}$ can be decomposed into two directions perpendicular to $\boldsymbol{m}$,

$$\delta \boldsymbol{s}_{\pm} = X_{\pm} \boldsymbol{m} \times \frac{d\boldsymbol{m}}{dt} + Y_{\pm} \frac{d\boldsymbol{m}}{dt}, \tag{1.26}$$

where $X_{\pm}$ and $Y_{\pm}$ are the spin-dependent constants and $d/dt = \partial/\partial t + \boldsymbol{v} \cdot \nabla$. The equation of motion for the electron-spin vector (1.25) is given by

$$\frac{d}{dt} \boldsymbol{s}_{\pm} = -\frac{2J_{\mathrm{ex}}}{\hbar} \boldsymbol{s}_{\pm} \times \boldsymbol{m} - \frac{\delta \boldsymbol{s}_{\pm}}{\tau_{\mathrm{sf}}}, \tag{1.27}$$

where τ_{sf} is the spin-flip relaxation time. The first term on the right-hand side of Eq. (1.27) is the Larmor precession of the electron spin around the magnetization axis. Conversely, the second term represents the spin relaxation describing the nonadiabatic dynamics of the electron spin. Substituting Eqs. (1.25) and (1.26) into Eq. (1.27), we obtain the following explicit expression for $X_{\pm}$ and $Y_{\pm}$:

$$X_{\pm} = \pm \frac{\hbar}{2J_{\mathrm{ex}}}, \quad Y_{\pm} = \pm \frac{\hbar}{2J_{\mathrm{ex}}} \frac{\hbar}{2J_{\mathrm{ex}}\tau_{\mathrm{sf}}}. \tag{1.28}$$

In the derivation of Eq. (1.28), the term $\partial \delta \boldsymbol{m}_{\pm}/\partial t$ is discarded because it gives a higher order term compared to the other terms. $X_{\pm}$ is $O(J_{\mathrm{ex}}^{-1})$ whereas $Y_{\pm}$ is $O(J_{\mathrm{ex}}^{-2})$. Substituting the obtained spin expectation value into Eq. (1.12), the spin electric field is given by

$$\boldsymbol{\mathcal{E}} = \frac{\hbar}{2e} (\boldsymbol{m} \times \dot{\boldsymbol{m}}) \cdot \nabla \boldsymbol{m} + \frac{\hbar}{2J_{\mathrm{ex}}\tau_{\mathrm{sf}}} \frac{\hbar}{2e} \dot{\boldsymbol{m}} \cdot \nabla \boldsymbol{m}. \tag{1.29}$$

The first term on the right-hand side of Eq. (1.29), which is equivalent to Eq. (1.22), comes from the adiabatic component $X_{\pm}$. The second term in Eq. (1.29), which goes to zero in the adiabatic limit $\tau_{\mathrm{sf}}/(\hbar J_{\mathrm{ex}}^{-1}) \to \infty$, comes from the nonadiabaticity in the

electron-spin dynamics and also depends on the spatial and temporal derivatives of the magnetization. By comparing Eqs. (1.24) and (1.29), we identify

$$\beta = \frac{\hbar}{2J_{\rm ex}\tau_{\rm sf}}. \tag{1.30}$$

When the spatial and temporal changes in the magnetization are parallel (i.e., $\dot{\boldsymbol{m}} \times \nabla \boldsymbol{m} = \boldsymbol{0}$), the nonadiabatic SMF becomes the leading term and the adiabatic SMF vanishes. Such a condition is fulfilled, for example, for a sliding DW motion in external fields less than the Walker breakdown field [17].

Experimentally, it is rather challenging to observe this nonadiabatic contribution to the SMF because the nonadiabatic parameter (1.30) is quite small, typically $\beta \sim 10^{-2}$. Currently, no measurement has been reported of this effect. One interesting proposal for its detection is to use the collective motion of a magnetic bubble array [41] to geometrically separate the adiabatic and nonadiabatic SMF and accumulate the SMF output from each bubble motion. A similar mechanism is anticipated in a lattice of skyrmions [40].

1.3.4 Spin-orbit coupling

In the previous subsections, we derived adiabatic and nonadiabatic contributions to the spin electric field, which depend on both $\dot{\boldsymbol{m}}$ and $\nabla \boldsymbol{m}$. Therefore, magnetic textures such as a DW or magnetic vortex are required. Note, however, that in a system with Rashba spin-orbit (SO) coupling [60] there exist additional spin electric fields even for uniform magnetization [32, 37, 39, 44].

In the nonrelativistic limit up to the order of $1/c^2$ (where c is the speed of light), the Hamiltonian of a conduction electron in a ferromagnetic conductor is

$$\mathcal{H} = \frac{\boldsymbol{p}^2}{2m_{\rm e}} + J_{\rm ex}\boldsymbol{\sigma}\cdot\boldsymbol{m} - \frac{e\eta_{\rm so}}{\hbar}\boldsymbol{\sigma}\cdot(\boldsymbol{p}\times\boldsymbol{E}). \tag{1.31}$$

In addition to the exchange interaction between electron spin and the magnetization, we introduce a SO interaction in the third term, with the SO coupling parameter $\eta_{\rm so} = \hbar^2/(4m_{\rm e}^2c^2)$ for the free-electron model (in real materials $\eta_{\rm so}$ can be enhanced by several orders of magnitude).

The velocity operator $\boldsymbol{v} = [\boldsymbol{r}, \mathcal{H}]/(i\hbar)$ is now given by

$$\boldsymbol{v} = \frac{\boldsymbol{p}}{m_{\rm e}} + \frac{e\eta_{\rm so}}{\hbar}\boldsymbol{\sigma}\times\boldsymbol{E}, \tag{1.32}$$

where the second term in the last line is the so-called anomalous velocity. The force $\boldsymbol{f}$ acting on the electron is given by Eq. (1.11), which is now extended as

$$\boldsymbol{f} = -J_{\rm ex}\boldsymbol{\sigma}\cdot\nabla\boldsymbol{m} + \frac{em_{\rm e}\eta_{\rm so}}{\hbar}\boldsymbol{\sigma}\times\dot{\boldsymbol{E}} + \frac{em_{\rm e}\eta_{\rm so}J_{\rm ex}}{\hbar}[\boldsymbol{\sigma}\times\boldsymbol{E}, \boldsymbol{\sigma}\cdot\boldsymbol{m}]. \tag{1.33}$$

The first term reproduces Eq. (1.11) whereas the second term originates from the time-derivative of the anomalous velocity. The third term is due to the noncommutative nature of the anomalous velocity and the exchange coupling. The expectation value of

the force $\boldsymbol{f}_\pm \equiv \langle \boldsymbol{k} \pm | \boldsymbol{f} | \boldsymbol{k} \pm \rangle$ is determined by the electron-spin dynamics [Eq. (1.27)]. Here we assume the condition $J_{\rm ex} \gg e\eta_{\rm so}|\boldsymbol{k}||\boldsymbol{E}|$, where the electron spin follows mostly the direction of $\mp\boldsymbol{m}$ due to the strong exchange coupling, whereas the SO interaction provides spin relaxation through the nonadiabatic spin-flip process.

The misalignment $\delta\boldsymbol{s}_\pm$ is again essential for $\boldsymbol{f}_\pm$. One can easily see that the values $\langle \boldsymbol{k} \pm | \boldsymbol{\sigma} \cdot \nabla \boldsymbol{m} | \boldsymbol{k} \pm \rangle$ and $\langle \boldsymbol{k} \pm | [\boldsymbol{\sigma} \times \boldsymbol{E}, \boldsymbol{\sigma} \cdot \boldsymbol{m}] | \boldsymbol{k} \pm \rangle$ appearing in the force are zero if $\boldsymbol{s}_\pm = \mp\boldsymbol{m}$. Substituting Eq. (1.26) with Eq. (1.28) into the expectation value of Eq. (1.33), we obtain $\boldsymbol{f}_\pm = \mp e\boldsymbol{\mathcal{E}}$, where the spin electric field reads

$$\boldsymbol{\mathcal{E}} = \frac{\hbar}{2e}(\boldsymbol{m} \times \dot{\boldsymbol{m}} + \beta\dot{\boldsymbol{m}}) \cdot \nabla \boldsymbol{m} + \frac{m_{\rm e}\eta_{\rm so}}{\hbar}\frac{\partial}{\partial t}(\boldsymbol{m} \times \boldsymbol{E}) + \beta\frac{m_{\rm e}\eta_{\rm so}}{\hbar}(\boldsymbol{m} \times \dot{\boldsymbol{m}}) \times \boldsymbol{E}. \quad (1.34)$$

Here we use Eq. (1.30) and the velocity-dependent terms are discarded for simplicity by considering an open circuit condition where the ensemble average of $\langle \boldsymbol{k} \pm | \boldsymbol{v} | \boldsymbol{k} \pm \rangle$ is zero. The first term in Eq. (1.34) comes purely from the exchange coupling and depends on $\nabla\boldsymbol{m}$, requiring nonuniform magnetization texture for the appearance of the SMFs as shown in the previous subsections. Conversely, the last two terms in Eq. (1.34), which contain the SO parameter $\eta_{\rm so}$, do not involve $\nabla\boldsymbol{m}$.

Kim *et al.* [32] showed that the spin electric field is proportional to $\dot{\boldsymbol{m}} \times \boldsymbol{E}$ and the resulting AC electric voltage can be produced in Rashba SO coupled systems, where the electric field $\boldsymbol{E}$ due to the inversion asymmetry is assumed to be static. This prediction was confirmed by FMR experiments in a ferromagnetic semiconductor (Ga,Mn)As [14]. Later, this contribution was found to be a part of a spin electric field proportional to $\partial(\boldsymbol{m} \times \boldsymbol{E})/\partial t$ [39], i.e., the third term in Eq. (1.34); an additional spin electric field proportional to $\boldsymbol{m} \times \dot{\boldsymbol{E}}$ appears. Note that, since the latter SMF can be induced with static and uniform magnetization, one can investigate the SMF electrically in detail with no disturbance arising from the inductive voltage, in contrast with the other SMF that lie at the origin of $\dot{\boldsymbol{m}}$. In addition, the SMF is tuned via the electric fields with variable frequencies [39, 45], whereas the time-dependence of the other SMFs is restricted by the characteristics of the magnetization dynamics. The fourth term reflects the nonadiabatic dynamics of electron spin and was derived in Rashba SO-coupled systems by elaborating the diagrammatic calculation by Tatara *et al.* [37]. The Onsager reciprocal relations between the charge current induced by Eq. (1.34) and the STT effects are discussed by Hals and Brataas [44]. Shibata and Kohno [23] also studied the SO-coupled ferromagnetic system (1.31) and predicted that the inverse Hall effect arises from the first term of Eq. (1.34).

1.3.5 Antiferromagnet

So far we have discussed the SMF only in ferromagnets. In this subsection, we consider a possibility of the SMF being generated in antiferromagnets (AFMs).

AFM spintronics is attracting more attention because of its potential to become a key player in technological applications where AFMs play an active role [61]. This motivates the demand for reliable methods to observe dynamical AFM textures that are often difficult to see directly by the conventional methods used in ferromagnet-based structures because of their small magnetization. SMFs, if present, would enable the detection of AFM dynamics by electrical means. Systems involving antiferromagnetic

resonance (AFMR) are good candidates for pursuing larger SMFs [9, 32] because the resonance frequencies are typically as high as terahertz.

Cheng and Niu [36] formulated a theory of electron dynamics in two-sublattice AFMs. One of their predictions is that no SMF appears unless a nonequilibrium spin polarization is introduced externally (e.g., by injecting spin into the AFM from an attached ferromagnet). This result is supported by the numerical research of Okabayashi and Morinari [42]. These two studies focus on the adiabatic contribution to SMF without SO couplings, which is an odd function of $\boldsymbol{m}$ and its sublattice average cancels out if the sublattice magnetizations are perfectly collinear.

In contrast, Ref. [46] shows that the nonadiabatic contribution to the SMF, which is even in $\boldsymbol{m}$, survives and becomes a leading contribution in textured AFMs. For example, the electric voltage induced by AFM DW motion is given by

$$V = -\frac{\hbar P \beta}{e\Delta} v_{\mathrm{DW}}, \tag{1.35}$$

where Δ is the DW width, and v_{DW} is the DW velocity. In addtion, the SO coupling contributions to the SMF remain. It is predicted that ac voltages are predicted to arise when the AFMR is excited in a Rashba SO system [46]. This effect would be more prominent for locally noncentrosymmetric AFM materials such as Mn_2Au and CuMnAs where the Rashba couplings are sublattice dependent and change its sign [62].

1.4 Experiments

In the previous section, we describe the origin of the SMF. In this section we review experiments for observing SMFs in DWs, pattered thin films, magnetic vortices, skyrmions, the Rashba SO-coupled systems, and magnetic nanoparticles.

1.4.1 Domain-wall motion in a ferromagnetic nanowire

As noted in § 1.2.2, the SMF was first measured in a setup of the field-induced DW motion in a permalloy nanowire by Yang *et al.* [7]. Here, we describe the real-time observation of SMF induced by DW motion by Hayashi *et al.* [11].

The experiment may be summarized as follows: First, we prepared permalloy nanowires (two samples with thickness of 20 nm and width of 300 and 600 nm) and attached electrodes to them for measuring voltage as shown in Fig. 1.4. Next, we created DWs in the permalloy nanowire by using a pulsed magnetic field and monitored with an oscilloscope the real-time voltage signals generated between the electrodes under an external constant magnetic field. The measurement sequence was repeated about 16000 times for different propagation directions of the DW (left or right) and different DW types: head-to-head (HH) or tail-to-tail (TT) DW, and the data in each of the four measurement conditions (Fig. 1.4) were averaged. The four combinations were measured to separate the contribution of the SMF and an inductive EMF generated in the measurement circuit. For the in-plane magnetization configuration, the negative (positive) magnetic charges are accumulated at both ends of the nanowire for a HH (TT) DW, whereas positive (negative) magnetic charges are concentrated around the DW region, giving rise to magnetic flux. Therefore, when a HH (TT) domain wall passes through the electrodes and enters the measurement circuit, the magnetic flux

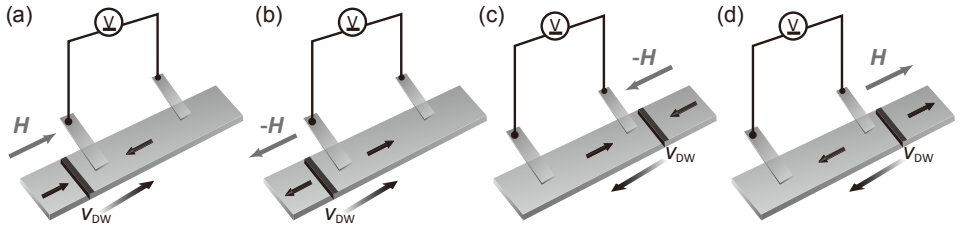

Fig. 1.4 Measurement setup for separating the inductive EMFs and SMFs. By changing the magnetic field directions (a), (c) HH-DW and (b), (d) TT-DW are led into the measurement circuit from the left and right, respectively.

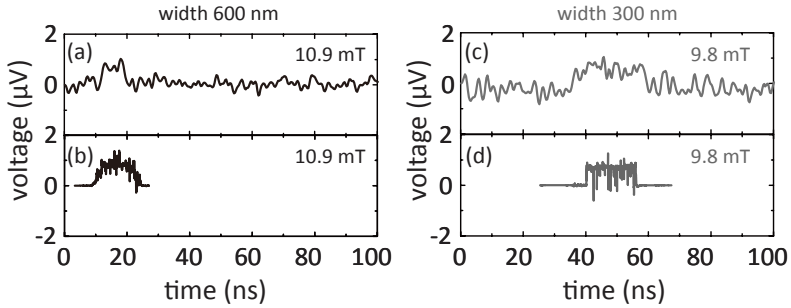

Fig. 1.5 Real time voltage signals due to DW motion [11]. Experimental data (a), (c), and numerical results (b), (d), for two nanowires with the wire width of 600 and 300 nm.

in the circuit increases (decreases), resulting in an inductive EMF in the circuit at that moment. Inversely, an inductive EMF in the opposite sense is measured when the DW leaves the circuit. This inductive EMF changes sign depending on the DW type but does not depend on the propagation direction of the DW. Conversely, the sign of the SMF is determined by the direction of the DW motion and is independent of the type of DW. Thus, the average of the *difference* between the output voltages for the TT and HH DWs driven by the same magnetic field is the inductive EMF whereas that of the *sum* corresponds to the SMF component.

Figure 1.5 shows the real-time voltage signal due to the SMF observed in the experiment together with the corresponding numerical results. We find that, for the external magnetic field, $\mu_0 H \sim 10$ mT, a dc voltage of about 1 μV appears in the time interval expected theoretically. When comparing the measurement results in nanowires of two different widths, the wider nanowire has the faster onset time and the shorter duration of the voltage signal. This result is attributed to the dependence of the DW speed on wire width (in permalloy nanowires, the DW mobility for magnetic fields is approximately proportional to the wire-width [3]).

This experiment confirms the following important theoretically predicted features of the SMF due to the field-induced DW motion: (1) The voltage drop occurs in the direction of the DW motion. (2) The SMF does not depend on the absolute value

of DW speed and its magnitude is determined by the magnetic field. Moreover, the numerical results based on the experimental parameters are consistent with the results of dc measurements.

1.4.2 Ferromagnetic resonance in a patterned thin film

The SMFs generated by the field-induced DW are intermittent because the voltage appears only during DW propagation between the two electrodes. For device applications, a continuous SMF was anticipated.

Yamane *et al.* [9] addressed this demand by using an asymmetrically patterned thin film. The sample is a comb-shape single permalloy film that consists of a wide flat pad and many wires as shown in Fig. 1.6(a) (see also Fig 1.1 for the setup). Relying on the difference in the shape magnetic anisotropy, the FMR is excited either in the wire or in the pad. As a result, the magnetization depends both on time and space and the conditions for generating the SMF are fulfilled. Figure 1.6(b) shows the output dc voltage as a function of microwave power in a permalloy thin film together with the corresponding numerical analysis.

A similar idea was employed by Nagata *et al.* [15] to excite a local FMR in a wedged thin film of a magnetite (Fe_3O_4) with negative spin polarization ($P < 0$). The observed voltage in Fe_3O_4 is opposite to that of permalloy with $P > 0$.

A dc voltage is generated by exciting the FMR in a lateral ferromagnetic/nonmagnetic (F/N) junction [63], which is explained by a spin pumping mechanism (i.e, the voltage is due to the spin accumulation at the F/N interface). In contrast, for the submillimeter-size comb sample, within which no well-defined interface exists, a negligibly small spin accumulation arises around the junction between the pad and wire, making it hard to explain this experiment in terms of the spin pumping.

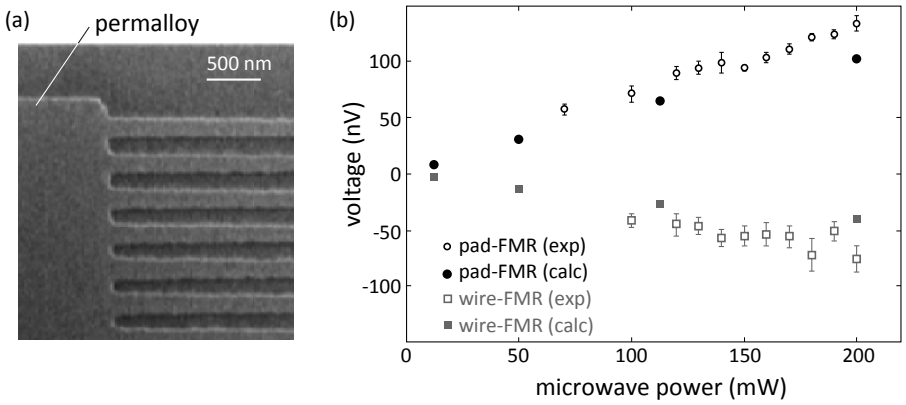

Fig. 1.6 Continuous SMF generation by FMR [9]. (a) A SEM image of the junction area of the comb shape permalloy thin film. (b) Output voltage as a function of microwave power. Black open (solid) circles represent experimental data (numerical results) for the FMR in the pad part, and gray open (solid) squares are the same for the FMR in the wire part.

1.4.3 Vortex core gyration in a magnetic disk

According to Eq. (1.22), rapid motion of a steep magnetization structure is favorable for generating a larger spin electric field. This is shown in Fig. 1.2(b), where a large potential difference appears locally around the complex magnetization structure. Such a situation can be more stably realized in the gyrating motion of a magnetic vortex core in a nanodisk. Upon applying an ac magnetic field, the core is resonantly excited. Calculations show that a sizable electric field of the order of kV/m appears in the direction perpendicular to the motion of the core [21]. The output voltage patterns patterns depend on the core polarization direction [21] and, with the aid of the Rashba SO coupling, even on the chirality [33], which can be used in possible spintronic devices to read out information coded in the core polarization and chirality.

Tanabe *et al.* [12] detected the ac voltage generated locally around the vortex core by attaching 100 nm electrodes to a permalloy disk with a diameter of 4.2μm. Again, the SMF and inductive EMF were separated with special care. The period of the voltage signal coincides with that of gyrating motion of the core, indicating that the observed voltage originates from the SMF associated with gyration of the vortex core.

1.4.4 Skyrmion lattice motion in chiral magnets

In chiral magnets such as MnSi and other B20 transition-metal compounds, skyrmion lattice phases arise as a new form of magnetic order with nonuniform magnetization texture. When the magnetization texture translates rigidly with the drift velocity $\boldsymbol{v}_{\rm d}$ as $\boldsymbol{m} \equiv \boldsymbol{m}(\boldsymbol{x} - \boldsymbol{v}_{\rm d}t)$, the time derivative is replaced by the space derivative: $\dot{\boldsymbol{m}} = -(\boldsymbol{v}_{\rm d} \cdot \nabla)\boldsymbol{m}$. The net force given by Eqs. (1.21)–(1.23) is then rewritten as $\boldsymbol{f}_{\pm} = \mp e(\boldsymbol{v}_k - \boldsymbol{v}_{\rm d}) \times \boldsymbol{\mathcal{B}}$, which induces the topological Hall effect provided that $\boldsymbol{v}_k \neq \boldsymbol{v}_{\rm d}$ [30].

Schulz *et al.* [10] prepared a skyrmion lattice in MnSin single crystals and drove skyrmion motion by applying electrical currents via the STT effect. They measured the Hall effect and found an excess component of the Hall voltage only when the skyrmions flowed along the current direction, confirming the predicted topological Hall effect. In contrast with the previous examples, which involved excitation by magnetic fields, the energy of the transverse voltage (SMF) in this experiment is supplied by the external current source and impurity potentials are essential for fulfilling the condition $\boldsymbol{v}_k \neq \boldsymbol{v}_{\rm d}$.

We note with interest that accumulating SMF outputs by using the skyrmion lattice [40] and similar structures [41] have been proposed. Furthermore, Shimada and Ohe [43] numerically studied the SMF induced by skyrmion dynamics in a confined geometry, taking into the edge effect.

1.4.5 Ferromagnetic resonance in a film with spin-orbit couplings

As noted, SMFs induced purely by the exchange interaction require magnetization textures ($\nabla \boldsymbol{m} \neq \boldsymbol{0}$). This requirement is relaxed when the SO coupling is introduced, as explained in §1.3.4. The effects of SO couplings generally become prominent in systems with the broken spatial inversion symmetry, such as (Ga,Mn)As and in heterostructures comprising ferromagnetic metals.

Ciccarelli *et al.* [14] excited the FMR in rectangular microbars of compressively strained (Ga,Mn)As via the STT effect by using ac currents, and then measured the ac voltages with a homodyne detection technique. The output voltages scale linearly

with respect to precession amplitude, as predicted in the previous section (1.3.4). The reciprocal relations between the STT and SMF [44] in this system were also examined.

1.4.6 Spin-flip tunneling in magnetic nanoparticles

By using molecular beam epitaxy, Hai *et al.* [8] fabricated a single-crystal magnetic tunnel device in which one of the electrodes consists of zinc-blende MnAs nanoparticles. They applied a static magnetic field to the device and observed the shift of the *I-V* curve indicating the generation of an effective EMF. The magnetization reversal of MnAs nanoparticles by the applied magnetic field derivers their Zeeman energy to conduction electrons via the SMF mechanism. In this system, the SMF effect combines with the Coulomb blockade effect that occurs in the nanoparticles, resulting in an extremely large magnetoresistance (MR) effect (MR ratio >100,000%) at low temperature.

Compared with typical magnetic textures such as DWs and vortices, systems of ferromagnetic nanoparticles have several advantages: the inductive EMFs need not be separated and the output voltage is quite large value (up to 22 mV). The key ingredient for the large output voltage is that nanoparticles simultaneously exhibit macroscopic quantum tunneling among the spin states together with spin-dependent tunneling through the nanoparticles. The requirement for such quantum tunneling phenomena is that the system should be cooled down to cryogenic temperature. If the device is regarded as a type of battery, the total power generated by the static magnetic field is proportional to the number of nanoparticles. In the experiment, the output lasts over several tens of minutes, whereas the estimated duration calculated from the total magnetic energy stored in the nanoparticles is only a few seconds [64]. In a quantum well of Al sandwiched by double spin-filtering EuS layers, Miao *et al.* [13] observed a similar long-lasting dc voltage output under static magnetic fields. These issues underscore the need for further investigation into the SMF in this system both experimentally and theoretically.

1.5 Applications

In this section, we briefly remark on some applied topics related to the SMF.

1.5.1 Dependence on materials

From Eq. (1.1), the output voltage of the SMF caused by DW motion is determined by the magnitude of applied magnetic fields apart from the spin polarization. However, as shown in the previous subsection, attempts to raise the output voltage by increasing the applied magnetic field lead to the structural deformation of a DWs in permalloy nanowires and result in the onset of high-frequency noise in the voltage signals. Given this situation, what principles guide the choice of materials for stabilizing a "large" SMF?

One answer to this question is to use ferromagnetic materials with a large magnetic anisotropy. In such materials, the DW is very "rigid" compared with permalloy and disturbance of the DW structure by the applied magnetic field is suppressed. Therefore, stable generation of SMFs even with a large magnetic field is expected.

For example, $L1_0$-ordered FePt and Co/Ni multilayer film are known for their large perpendicular magnetic anisotropy. Numerical simulation [31] shows that stable DW motion can occur in the range of several hundred mT for a Co/Ni multilayer nanowire and up to several T for a FePt nanowire. With such magnetic fields, the Co/Ni shows tens of microvolts, and the FePt is expected to reach hundreds of microvolts, which is about 100 times larger than those reported in the permalloy samples so far. Moreover, DWs in these materials are narrow and have relatively low DW mobility. These properties are also advantageous in terms of downsizing of devices that use SMFs.

1.5.2 Shape effect

For the SMF introduced so far, external magnetic fields are used to drive DWs. Considering the spin electric field (1.22), however, one can see that it does not matter what causes the magnetization dynamics. For example, a DW has a certain surface energy, which is proportional to the cross-sectional area of a magnetic nanowire [65]. Therefore, in a magnetic nanowire with a nonuniform cross-sectional area, a DW moves spontaneously in the direction in which the DW energy is lowered (i.e., the cross-sectional area decreases). In such a nonuniform magnetic nanowire, the generation of voltages originating from the internal magnetic energy of the ferromagnet can be expected without requiring an external magnetic field.

To demonstrate this idea, numerical simulations of a shaped permalloy nanowire were done [29]. The DW was found to move spontaneously in a region where the wire width tapers off without the aid of an external magnetic field and, in turn, the SMF signals of several microvolts were obtained. This result indicates that the internal magnetic energy stored in the DW of ferromagnetic materials may be used for generating an EMF and its output characteristic can be controlled by nanoprocessing of the wire shape. Magnetic nanodevices such as a memory elements and current amplifiers have been proposed based on this concept [4].

Another porposal is to use the shape effect in a "magnetic power inverter," [34], which is a device that converts dc magnetic fields to ac electric voltages. This device consists of a magnetic nanowire with the width modulation. In such a patterned wire, a DW behaves like an elastic membrane and the DW energy varies as a function of the DW position. Accordingly, a DW introduced in the nanowire is subjected not only to an applied dc magnetic field but also to an effective magnetic field arising from the modulation of the DW energy and that is proportional to the wire width. In this case, the output voltage has an ac component that reflects the alternating DW energy in addition to a normal dc component due to the input static magnetic field. Characteristics of the ac component such as amplitude (several μV) and frequency (MHz to GHz) can be tuned by design of the wire shape, choice of materials, and magnitude of applied static magnetic fields.

1.6 Summary and outlook

We have seen that the SMF is induced in magnetic nanostructures via the exchange interaction between conduction spin and magnetization. Various types of the spin electric fields are possible: adiabatic, nonadiabatic, and their SO coupled equivalents. In experiment, the adiabatic contributions with/without SO coupling have been observed

whereas detecting nonadiabatic effects is challenging. The SMF offers electrical detection of magnetization dynamics, which would allow us to monitor the elusive dynamics of antiferromagnets.

In spintronics applications, the current drive is to obtain higher performance of existing devices, such as magnetic memory, magnetic head, and magnetic sensors, has been pursued so far. Today they are widely recognized as promising candidates for ultimate "energy-saving" technology. Additionally, SMF introduces the basic concept of "energy-harvesting" technology in spintronics and opens a new pathway to the conversion between magnetic and electric energy by using magnetic materials.

In contrast, the magnitude of the SMF realized so far is limited to at most a few microvolts at room temperature. For practical use, the weakness of the output voltage signals remains a major challenge. To solve this problem, two directions may be pursued: The first is to elucidate the SMF-amplification mechanism in the systems of magnetic nanoparticles, as discussed in §1.4.6. The second is to regard the SMF as an effective change in resistance rather than as a voltage signal. The former provides an interesting research theme in condensed matter physics and the latter can be applied to magnetic heads and high-sensitivity magnetic sensors.

Acknowledgements

The authors thank S. E. Barnes, D. Chiba, P. N. Hai, M. Hayashi, H. W. Lee, S. Mitani, J. Ohe, T. Ono, K. Sasage, E. Saitoh, J. Sinova, K. Tanabe, M. Tanaka, and Y. Yamane for collaboration and G. E. W. Bauer, H. Fukuyama, M. Kläui, H. Kohno, J. Shibata, and G. Tatara for useful discussions. This work is supported by Grant-in-Aids for Scientific Research (No. 24740247, 26247063, and 16K05424) from MEXT, Japan and also by ERATO Saitoh Spin Quantum Rectification Project from Japan Science and Technology Agency.

References

[1] J. C. Slonczewski, J. Magn. Magn. Mater. **159**, L1 (1996).
[2] L. Berger, Phys. Rev. B **54**, 9353 (1996).
[3] See Chapter 23 and G. S. D. Beach, M. Tsoi, J. L. Erskine, J. Magn. Magn. Mater. **320**, 1272 (2008).
[4] S. E. Barnes, J. Ieda, and S. Maekawa, Appl. Phys. Lett. **89**, 122507 (2006).
[5] A. Stern, Phys. Rev. Lett. **68**, 1022 (1992).
[6] S. E. Barnes and S. Maekawa, Phys. Rev. Lett. **98**, 246601 (2007).
[7] S. A.Yang, G. S. D. Beach, C. Knutson, D. Xiao, Q. Niu, M. Tsoi, and J. L. Erskine, Phys. Rev. Lett. **102**, 067201 (2009).
[8] P. N. Hai, S. Ohya, M. Tanaka, S. E. Barnes, and S. Maekawa, Nature **458**, 489 (2009).
[9] Y. Yamane, K. Sasage, T. An, K. Harii, J. Ohe, J. Ieda, S. E. Barnes, E. Saitoh, and S. Maekawa, Phys. Rev. Lett. **107**, 236602 (2011); *ibid.* **113**, 179901 (2014).
[10] T. Schulz, R. Ritz, A. Bauer, M. Halder, M. Wagner, C. Franz, C. Pfleiderer, K. Everschor, M. Garst, and A. Rosch, Nature Phys. **8**, 301 (2012).
[11] M. Hayashi, J. Ieda, Y. Yamane, J. Ohe, Y. K. Takahashi, S. Mitani, and S. Maekawa, Phys. Rev. Lett. **108**, 147202 (2012).
[12] K. Tanabe, D. Chiba, J. Ohe, S. Kasai, H. Kohno, S. E. Barnes, S. Maekawa, K. Kobayashi, T. Ono, Nature Commun. **3**, 845 (2012).
[13] G. X. Miao, J. Chang, B. A. Assaf, D. Heiman, and J. S. Moodera, Nature Commun. **5**, 3682 (2014).
[14] C. Ciccarelli, K. M. D. Hals, A. Irvine, V. Novak, Y. Tserkovnyak, H. Kurebayashi, A. Brataas, and A. Ferguson, Nature Nanotechnol. **10**, 50 (2015).
[15] M. Nagata, T. Moriyama, K. Tanabe, K. Tanaka, D. Chiba, J. Ohe, Y. Hisamatsu, T. Niizeki, H. Yanagihara, E. Kita, and T. Ono, Appl. Phys. Exp. **8**, 123001 (2015).
[16] W. M. Saslow, Phys. Rev. B **76**, 184434 (2007).
[17] R. A. Duine, Phys. Rev. B **77**, 014409 (2008).
[18] M. Stamenova, T. N. Todorov, and S. Sanvito, Phys. Rev. B **77**, 054439 (2008).
[19] Y. Tserkovnyak and M. Mecklenburg, Phys. Rev. B **77**, 134407 (2008).
[20] Y. Tserkovnyak and C. H. Wong, Phys. Rev. B **79**, 014402 (2009).
[21] J. Ohe and S. Maekawa, J. Appl. Phys. **105**, 07C706 (2009); J. Ohe, S. E. Barnes, H. W. Lee, and S. Maekawa, Appl. Phys. Lett. 95, 123110 (2009).
[22] S. Zhang and S. S.-L. Zhang, Phys. Rev. Lett. **102**, 086601 (2009).
[23] J. Shibata and H. Kohno, Phys. Rev. Lett. **102**, 086603 (2009).
[24] S. A.Yang, G. S. D. Beach, C. Knutson, D. Xiao, Z. Zhang, M. Tsoi, Q. Niu, A. H. MacDonald, and J. L. Erskine, Phys. Rev. B **82**, 054410 (2010).
[25] S. S.-L. Zhang and S. Zhang, Phys. Rev. B **82**, 184423 (2010).

[26] M. E. Lucassen, G. C. F. L. Kruis, R. Lavrijsen, H. J. M. Swagten, B. Koopmans, and R. A. Duine, Phys. Rev. B **84**, 014414 (2011).
[27] J. Shibata and H. Kohno, Phys. Rev. B **84**, 184408 (2011).
[28] Y. Yamane, J. Ieda, J. Ohe, S. E. Barnes, and S. Maekawa, J. Appl. Phys. **109**, 07C735 (2011).
[29] Y. Yamane, J. Ieda, J. Ohe, S. E. Barnes, and S. Maekawa, Appl. Phys. Exp. **4**, 093003 (2011).
[30] J. Zang, M. Mostovoy, J. H. Han, and N. Nagaosa, Phys. Rev. Lett. **107**, 136804 (2011).
[31] Y. Yamane, J. Ieda, and S. Maekawa, Appl. Phys. Lett. **100**, 162401 (2012).
[32] K. W. Kim, J. H. Moon, K. J. Lee, and H. W. Lee, Phys. Rev. Lett. **108**, 217202 (2012).
[33] J. H. Moon, K. W. Kim, H. W. Lee, and K. J. Lee, Appl. Phys. Exp. **5**, 123002 (2012).
[34] J. Ieda and S. Maekawa, Appl. Phys. Lett. **101**, 252413 (2012).
[35] J. Kishine, I. G. Bostrem, A.S. Ovchinnikov, and Vl. E. Sinitsyn, Phys. Rev. B **86**, 214426 (2012).
[36] R. Cheng and Q. Niu, Phys. Rev. B **86**, 245118 (2012).
[37] G. Tatara, N. Nakabayashi, and K. J. Lee, Phys. Rev. B **87**, 054403 (2013).
[38] J. Ieda, Y. Yamane, and S. Maekawa, J. Korean Phys. Soc. **62**, 1802 (2013).
[39] Y. Yamane, J. Ieda, and S. Maekawa, Phys. Rev. B **88**, 014430 (2013).
[40] J. Ohe and Y. Shimada, Appl. Phys. Lett. **103**, 242403 (2013).
[41] Y. Yamane, S. Hemmatiyan, J. Ieda, S. Maekawa, and J. Sinova, Sci. Rep. **4**, 6901 (2014).
[42] A. Okabayashi and T. Morinari, J. Phys. Soc. Jpn **84**, 033706 (2015).
[43] Y. Shimada and J. Ohe, Phys. Rev. B **91**, 174437 (2015).
[44] K. M. D. Hals and A. Brataas, Phys. Rev. B **91**, 214401 (2015).
[45] C. S. Ho, M. B. A. Jalil, and S. G. Tan, New J. Phys. **17**, 123005 (2015).
[46] Y. Yamane, J. Ieda, and J. Sinova, Phys. Rev. B **93**, 180408(R) (2016).
[47] V. Korenman, J. L. Murray, and R. E. Prange, Phys. Rev. B **16**, 4032 (1977).
[48] G. E. Volovik, J. Phys. C **20**, L83 (1987).
[49] L. Berger, Phys. Rev. B **33**, 1572 (1986).
[50] J. Ieda, Y. Yamane, and S. Maekawa, SPIN **03**, 1330004 (2013).
[51] T. Fujita, M. B. A. Jalil, S. G. Tan, and S. Murakami, J. Appl. Phys. **110**, 121301 (2011).
[52] D. J. Griffiths, Chapter 10 in *Introduction to Quantum Mechanics 2nd ed.* (Pearson Education Inc., Upper Saddle River 2005).
[53] M. Yamanaka, W. Koshibae, and S. Maekawa, Phys. Rev. Lett. **81**, 5604 (1998).
[54] J. Ye Y. B. Kim, A. J. Millis, B. I. Shraiman, P. Majumdar, and Z. Tešanović, Phys. Rev. Lett. **83**, 3737 (1999).
[55] Y. Taguchi, Y. Oohara, H. Yoshizawa, N. Nagaosa, and Y. Tokura, Science **291**, 2573 (2001).
[56] N. Nagaosa, J. Phys. Soc. Jpn **75**, 042001 (2006).
[57] http://math.nist.gov/oommf/.
[58] K. Yu. Bliokh and Yu. P. Bliokh, Annals Phys. **324**, 13 (2005).

[59] Y. Yamane, J. Ieda, and J. Sinova, Phys. Rev. B **94**, 054409 (2016).
[60] A. Soumyanarayanan, N. Reyren, A. Fert, and C. Panagopoulos, Nature **539**, 509 (2016).
[61] T. Jungwirth, X. Marti, P. Wadley, and J. Wunderlich, Nature Nanotechnol. **11**, 231 (2016).
[62] J. Železný H. Gao, K. Výborný, J. Zemen, J. Mašek, A. Manchon, J. Wunderlich, J. Sinova, and T. Jungwirth, Phys. Rev. Lett. **113**, 157201 (2014).
[63] M. V. Costache, M. Sladkov, S. M. Watts, C. H. van der Wal, and B. J. van Wees, Phys. Rev. Lett. **97**, 216603 (2006).
[64] D. C. Ralph, Nature **474**, E6 (2011).
[65] J. Ieda, H. Sugishita, and S. Maekawa, J. Magn. Magn. Mater. **322**, 1363 (2010).